NC

17

Quarterly Summary Report No. 2
Spectroscopic Investigations of Plasma Properties
(11 August — 10 November 1964)

Contract No. NASw-922

Engineering Department Report No. 4038

Allison Division • General Motors

Indianapolis, Indiana

Quarterly Summary Report No. 2
Spectroscopic Investigations of Plasma Properties
(11 August — 10 November 1964)

Contract No. NASw-922

Engineering Department Report No. 4038

9 December 1964

R. T. Schneider
Project Manager

F. G. Myers
Director of Research

TABLE OF CONTENTS

LIST OF ILLUSTRATIONS

SUMMARY

23211

The performance of the plasma source operated with helium is described. Intensity and temperature profiles of the source are included. A picture of the source taken in the light of different lines is shown. The dependency of the core temperature of the arc on the arc current is shown. The electronic instrumentation for detecting weak spectrum lines is described.

Author

I. INTRODUCTION

This program consists essentially of three phases. The first phase is the development of a plasma source in which electron density and temperature can be adjusted over a reasonable range. It is planned to do this with a helium arc, seeded with a predetermined amount of cesium. The second phase is the development of electronic instrumentation to detect weak spectrum lines. Finally, the third phase is the measurement of the temperature of the plasma source with different spectroscopic temperature measurement methods and the comparison of the results with the results of a new temperature measurement method, to be developed during the program. Also in the third phase, the line broadening of the cesium lines, caused by the Stark effect, will be measured as a function of the electron density, using the electronic instrumentation to detect weak lines.

The first quarterly report[1]* described the new method for temperature measurement and the design and construction of the plasma source. This second quarterly report describes the performance of the plasma source operating with helium alone. Also, the performance of the electronic instrumentation for detection of weak lines is discussed.

The third quarterly report will be devoted to a description of the performance of the plasma source when operating with a helium-cesium mixture. The final report will contain the results in the form of temperature measurements and electron density measurements.

Work during the second quarter was performed by W. Woerner, R. O. Whitaker, and Dr. R. T. Schneider.

*Superscript numbers refer to references in Section VI.

II. EXPERIMENTAL ARRANGEMENT

The design and construction of the experimental plasma source was described in the first quarterly report.[2] It has not been necessary to change the design during the program to date.

It is well known that helium is not a convenient gas in which to operate an arc. Helium tends to form a very instable arc; therefore, it was necessary to study the short-time behavior of the discharge. For this purpose, high-speed movies of the arc were taken with a Fastax camera. The maximum applied film speed was 6000 frames/sec. Figure 1a shows 20 frames of this film. These pictures show that the arc is pulsating at a frequency of approximately 120 cps. Although the pulsation may appear blurred in Figure 1a, it can be seen clearly when projecting the film in a movie projector. The same pulsation can be detected when monitoring the light output of the arc with a photomultiplier, as shown in Figure 2 (lower beam). The fine structure of the signal is caused by the chopping frequency of the light chopper and does not constitute additional information. On the upper beam of Figure 2, the arc current is monitored. Although the spectroscopic power supply used has only a small ripple, operation with the arc causes the large fluctuations of the light output and of the arc shape. Therefore, a special motor generator set with electronic stabilization was used. The light output of the arc then remained constant and no ripple could be detected on the arc current. The shape of the improved arc is shown in Figure 1b. No fluctuations are visible in Figure 1b, although it should be noted that the shape of the arc has changed considerably.

The arc in its improved form is suitable for spectroscopic study.

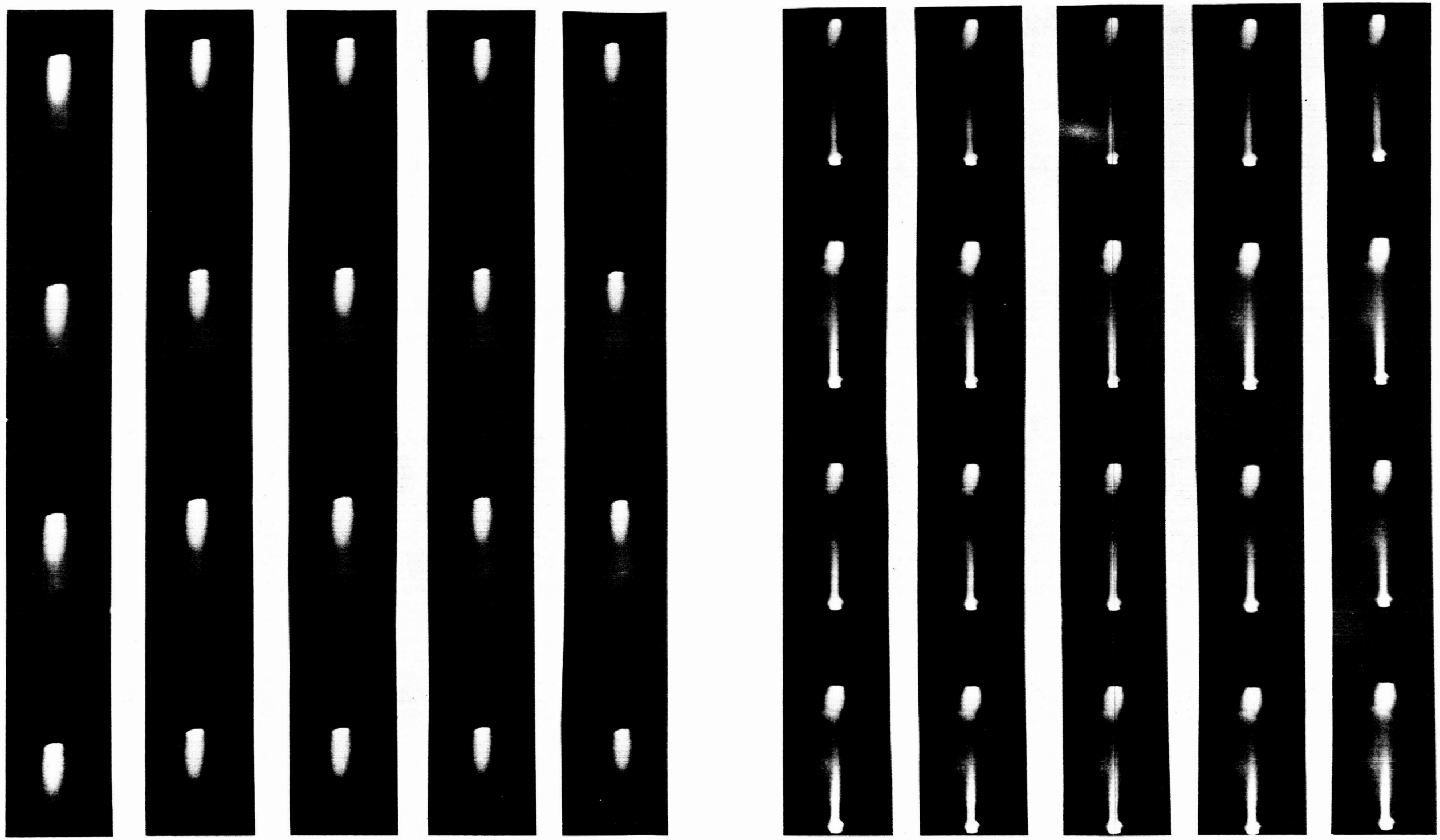

Figure 1. High-speed movies of a helium arc, showing fluctuating and improved arcs.

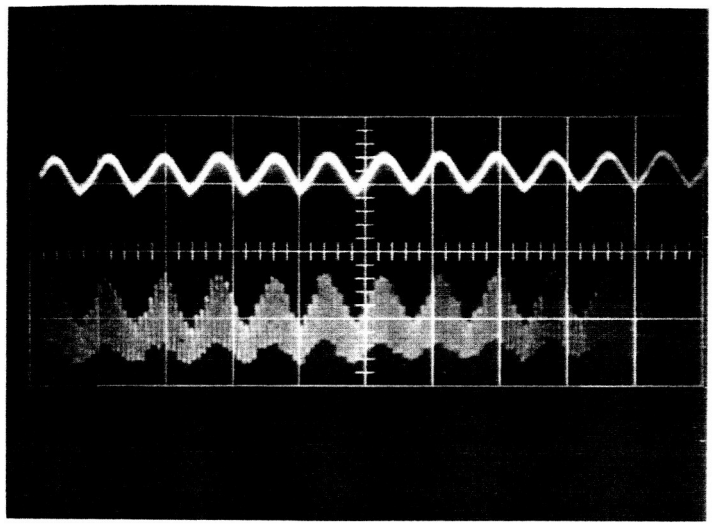

Figure 2. Arc current and light output of the helium arc – deflection: 10 msec/cm.

III. INTENSITY PROFILES AND TEMPERATURE DETERMINATION

ABEL INVERSION

The intensity, $i_\lambda(\vec{r})$, of a spectral line of wavelength λ is defined as the energy of photons of wavelength λ emitted per unit time from a unit volume around the point $\vec{r} = \{x, y, z\}$ of the radiation source. Due to the spatial extension of actual radiation sources like radiating plasmas, the local quantity $i(\vec{r})$—the subscript λ is omitted herein for simplicity—cannot generally be observed directly by means of a spectrograph.

Consider a radiation source of cylindrical symmetry which is typical for arc radiation sources. Introducing cylindrical coordinates (r, θ, z), the intensity is then only a function of radius, $i = i(r)$. For this geometry, an intensity, $I(x)$, is observed by means of the spectrograph which depends only on the slit coordinate x, designating the position of the spectrograph relative to the source. The intensity $I(x)$ represents energy emitted from the plasma slab of width $\Delta x = 1$, depth $\Delta y = 2\, y_o$, and height $\Delta z = 1$. Designating the radius of the cylindrical source as R, the half depth is given by $y_o = \sqrt{R^2 - x^2}$.

Assuming that the plasma is optically thin, it may be seen from Figure 3a that the observed intensity, $I(x)$, is related to the true intensity, $z(r)$ (because x is kept constant, it is $dy = r\, d\, r/\sqrt{r^2 - x^2}$) by:

$$I(x) = \int_{-y_o}^{+y_o} i(r)\, dy = 2 \int_{x}^{R} \left[i(r)\, r/\sqrt{r^2 - x^2} \right] dr \qquad (1)$$

From this integral equation the true intensity may be obtained explicitly by means of Abel's transformation:[3]

$$i(r) = -(1/\pi) \int_{r}^{R} \left[I'(x)/\sqrt{x^2 - r^2} \right] dx \qquad (2)$$

$$I'(x) \equiv dI(x)/dx$$

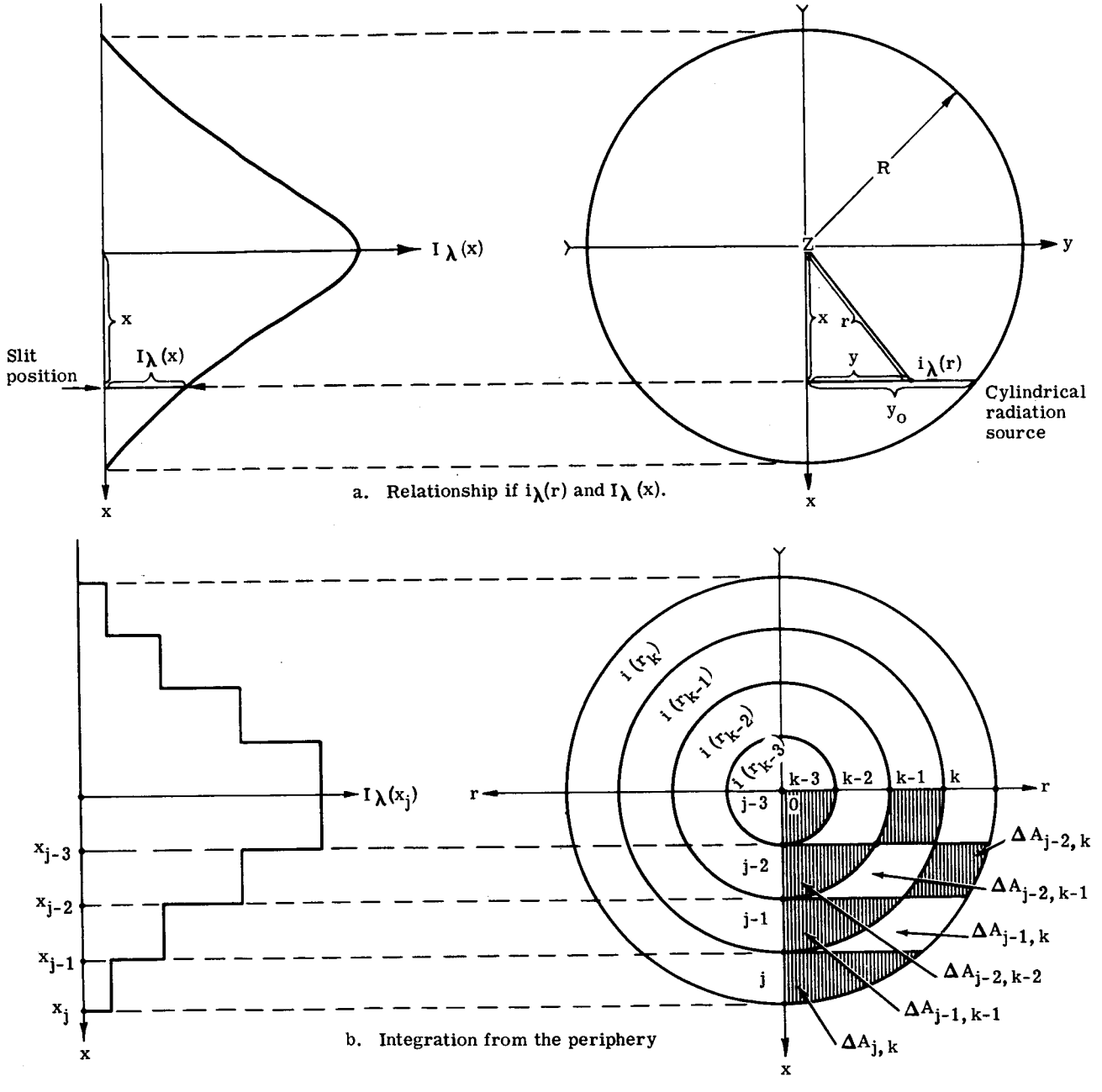

Figure 3. Cylindrical radiation source.

The integral of Equation (2) cannot generally be solved analytically due to the nonelementary form of the experimentally determined I(x) and I'(x) curves. For this reason, it is suitable to integrate Equation (1) numerically[4,5] if it is assumed that the plasma is optically thin.

To understand the numerical method, imagine first that the true intensity distribution, i(r), is approximated by a step function of the radius, $i(r_{k-n})$, with a finite number of steps (k) as shown in Figure 3b (the integer n lies in the interval $0 \leq n \leq k-1$). The number of rings, k, is chosen so that within each ring the intensity $i(r_{k-n})$ can be regarded as sufficiently constant. In addition to the index k, which designates the position upon the radius r, another index, j, is introduced to denote the position on the x axis.

The true intensity in the outer ring, $i(r_k)$, is related to the observed intensity, $I(x_j)$—obtained at the corresponding slit position, x_j—by:

$$i(r_k)\ 2\ \Delta\ A_{j,k} = I(x_j) \tag{3}$$

The true intensity in the second ring, $i(r_{k-1})$, referenced from the periphery, is related to the observed intensities, $I(x_{j-1})$ and $I(x_j)$, by:

$$i(r_{k-1})\ 2\ \Delta\ A_{j-1,k-1} = I(x_{j-1}) - i(r_k)\ 2\ \Delta\ A_{j-1,k} \tag{4}$$

where $i(r_k)$ is to be considered as known from Equation (3).

The true intensity in the third ring, $i(r_{k-2})$, referenced from the periphery, is related to the observed intensities $I(x_{j-2})$, $I(x_{j-1})$, and $I(x_j)$, by:

$$i(r_{k-2})\ 2\ \Delta\ A_{j-2,k-2} = I(x_{j-2}) - i(r_{k-1})\ 2\ \Delta\ A_{j-2,k-1} - i(r_k)\ 2\ \Delta\ A_{j-2,k} \tag{5}$$

Thus, for the true intensity in the nth ring, referenced from the periphery:

$$i(r_{k-n})\ 2\ \Delta\ A_{j-n,k-n} = I(x_{j-n}) - i(r_{k-[n-1]})\ 2\ \Delta\ A_{j-n,k-[n-1]} - i(r_{k-[n-2]})\ 2\ \Delta\ A_{j-n,k-[n-2]} - \ldots - i(r_k)\ 2\ \Delta\ A_{j-n,k} \tag{6}$$

The areas $\Delta\ A_{j-s,k-r}$ are pure geometrical quantities and are given explicitly by Pearce.[6] By means of Equation (6)—starting at the periphery (n = 0)—the true intensity step profile, $i(r_k), \ldots, i(r_1)$ can be calculated from the observed intensity step profile, $I(x_j), \ldots, I(x_1)$.

INTENSITY AND TEMPERATURE PROFILE OF HELIUM ARC

The two methods of temperature determination used in this program to date are the line intensity ratio method and the absolute line intensity method. Although the line intensity ratio method is more convenient, the absolute intensity method is potentially more sensitive, since the absolute intensity of a spectrum line varies more with temperature than does the ratio of the line intensities of the spectrum. For the absolute method the photographic plate or electronic instrumentation must be calibrated with a known light source positioned at the same or optically equivalent place as the plasma. Furthermore, the thickness of the plasma layer emitting the spectrum line must be known. With the ratio method, average plasma temperatures can be obtained without knowing the thickness of the emitting layers, assuming that the spectrum lines compared are emitted from the same layers. For a plasma with a temperature profile this is not true, however, since spectrum lines originating from transitions from higher energy levels are emitted from a smaller volume of the plasma than are spectrum lines with low upper energy levels. Thus, for more accurate temperature measurements with the line ratio method, the relative distribution of the emission of those spectrum lines in the plasma which are used must be determined. For plasmas with cylindrical symmetry, such as the arc under consideration, the radial distribution of the radiation can be derived from the observed side-on intensities by the Abel integration as described previously. The arc is photographically recorded in the plane of the entrance slit of the spectrograph, with the arc axis perpendicular to the slit. The spectrum lines then represent a side-on profile of the section cut out by the spectrograph entrance slit seen in the light of the different wavelengths.

An approximate determination of the arc core temperature can be made by measuring the photographic density at the corresponding portion of two spectrum lines with different upper energy levels. For the work reported herein, the following helium lines were used: $3^3S \rightarrow 2^3P$ ($\lambda = 7065\text{Å}$) and $5^3D \rightarrow 3^3P$ ($\lambda = 4026\text{Å}$). By noting the difference in photographic densities, the difference in the source intensities can be calculated. From the ratio of these intensities, the temperature may be derived. When more than one spectrum line is used, the method becomes more accurate. The intensities of the different lines, plotted over the energy levels of the upper states, should yield a straight line with 1/T as slope. The fact that the measured points lie on a straight line is also a proof of thermal equilibrium.

Figure 4 shows the results of such measurements on a 5- and 10-amp arc. However, to determine the exact arc core temperatures, the relative radial intensity distribution of the used spectrum lines must be known, which means that the Abel inversion must be applied. Figure 5 shows the relative radial intensity distribution for the lines $\lambda = 7065\text{Å}$ and $\lambda = 4026\text{Å}$ in a 7.5-amp arc after the Abel inversion. It will be noted that the ratio I_{7065}/I_{4026} decreases with

increasing radius, indicating a temperature minimum in the arc center. Similar results have been noted by other experimenters[7,8] and were explained by the absence of thermal equilibrium or by scattered light in the spectrograph. In this case, the reason appears to be that the γ factor of the photoplates was not constant. The S-shaped curve of the D-log E curve is well known, and it is evident that the value of γ does not remain constant in the lower density region. Because in this region photographic recording is most sensitive, the D-log E curve was transformed as described by Seidel into a W-log E curve,[9] which extends the region of constant γ factor to lower exposures. However, the W-log E curves are not equally suitable for all wavelengths. For the two red lines (λ = 7065Å and λ = 6678Å), the γ factor (the slope of the curves) remains constant over the entire region. This is not the case for other lines, however, and

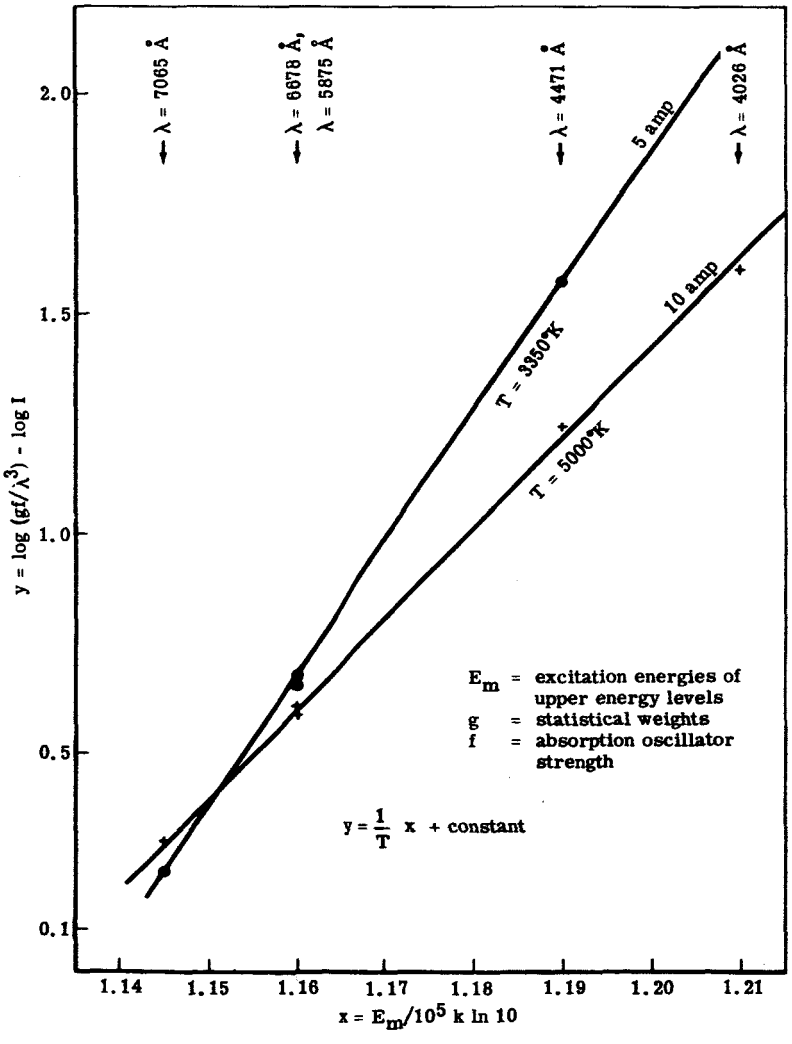

Figure 4. Temperature determination for 10- and 5- amp helium arc.

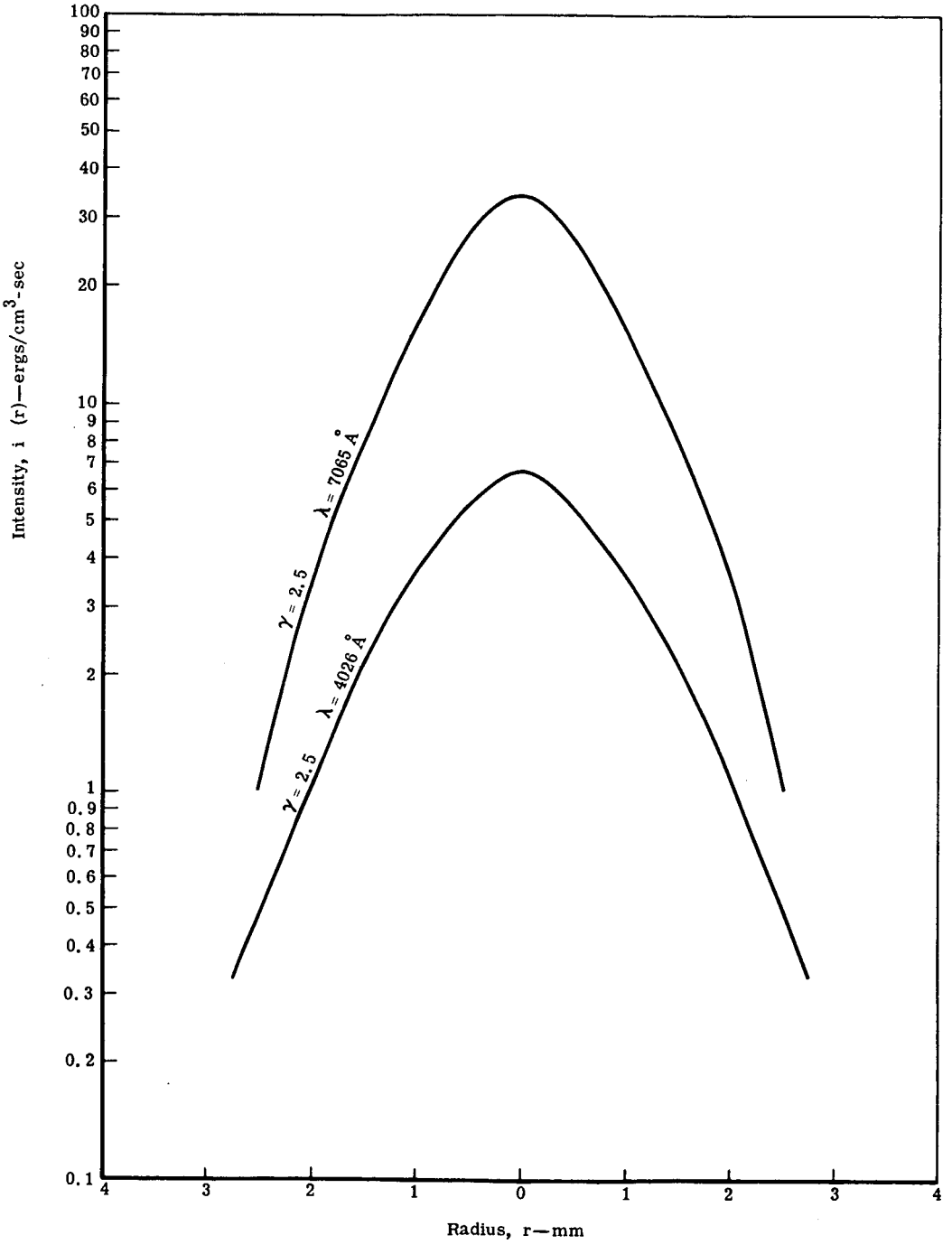

Figure 5. Intensity profile for λ = 7065 and 4026 Å.

must be considered when working with these lines. In most cases, error due to improper values may go undetected, but they might lead to completely wrong results in determining temperature profiles with the line ratio method. Because the ratio of line intensities is a rather weak function of the temperature, errors in the intensity determination have a relative large influence. Therefore, it is more adequate to determine only the core temperature with the line ratio method and to derive the remainder of the profile from the core temperature, using the radial intensity distribution of single lines. Such temperature profiles are shown in Figure 6. The profile is derived from the intensity profiles in Figure 5. Since it is the same arc, the temperature profiles derived by using the lines $\lambda = 7065$ Å and $\lambda = 4026$ Å should be identical.

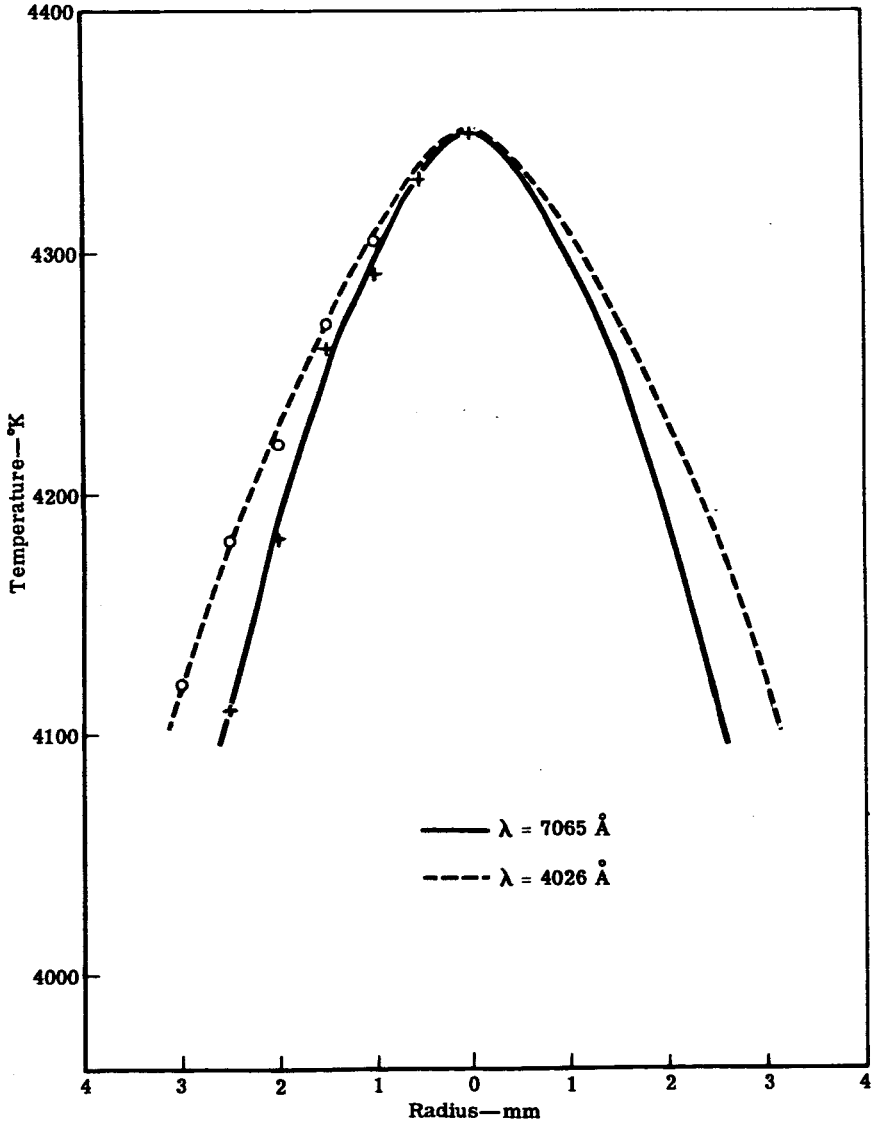

Figure 6. Temperature profile of helium arc at 7. 5 amp.

The difference apparently occurs because the γ value of the plate is not constant over the entire density range used. Since, in measuring intensity profiles of an arc, a large region of intensities must be covered, it seems worthwhile to investigate the influence of varying γ factor on intensity profiles derived by the Abel integration. The first step was to insert γ into the computer as a function of photographic density. As Figure 7 shows, the profiles are different from those in Figure 5. But the ratio I_{7065}/I_{4026} still has a maximum in the arc center, indicating that the adjustment was not adequate. Figure 8 shows that the proper adjustment would be γ as a function of density (or the W values, respectively) and of wave length. The proper adjustment could also be determined by finding a function, F-log E, that is a straight line for all wavelengths used in the photographic density ranges. In general spectrographic work, error is avoided—due to nonlinearity of the response of the photographic emulsions—by comparing spectrum lines with small differences in wavelengths and adjusting the exposures (for instance, by the use of step filters) to obtain approximately the same density on the photo plate for the compared lines. These conditions, however, cannot be fulfilled in the Allison case; it is, therefore, worthwhile to investigate the effect of the nonlinearity of the photographic response on temperature profiles deduced by the Abel inversion. This result will be reported in a subsequent report.

Figure 9 shows the dependency of arc core temperature on arc current. The temperature was taken in the arc column, halfway between the anode and the cathode.

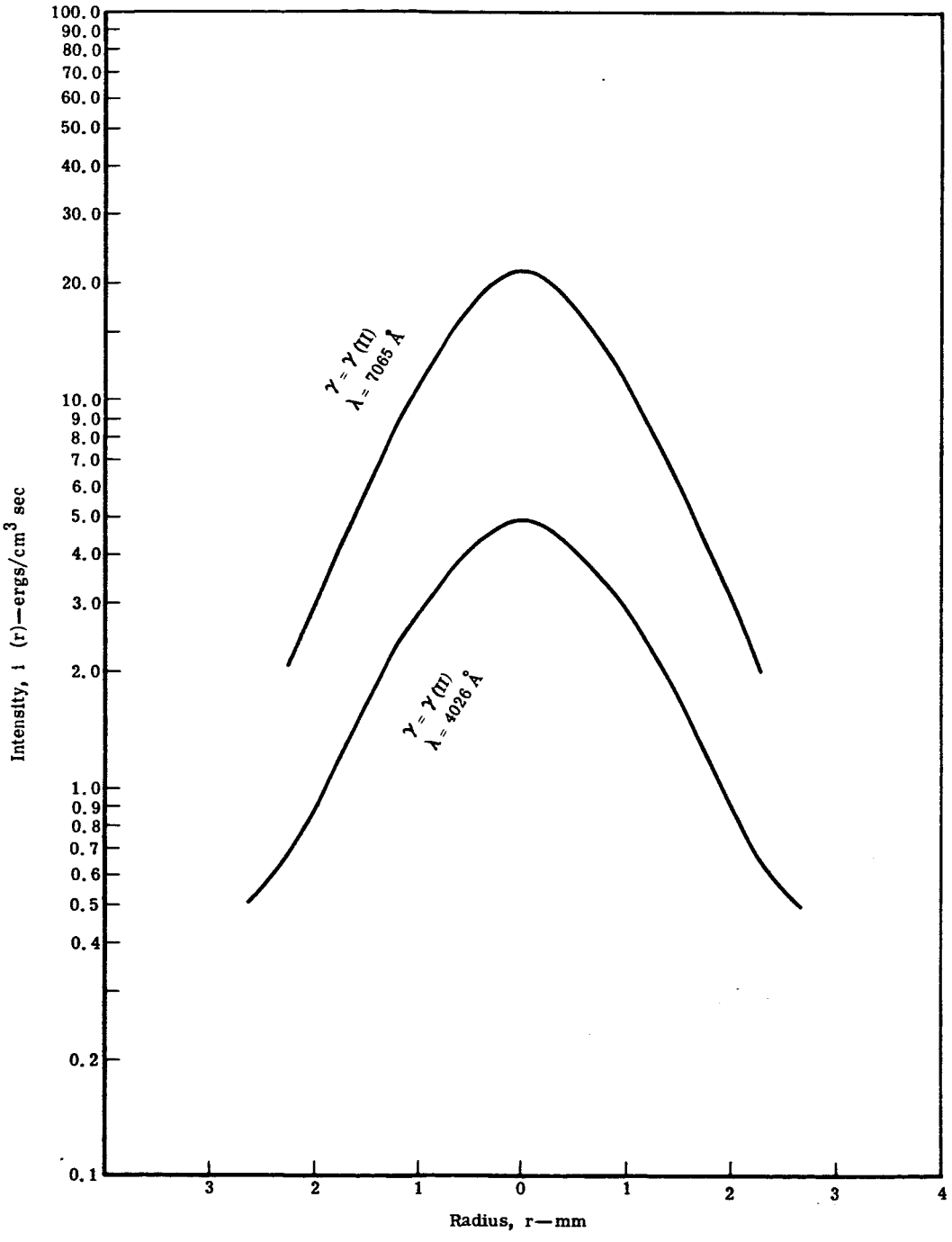

Figure 7. Adjusted intensity profile for λ = 7065 and 4026 Å.

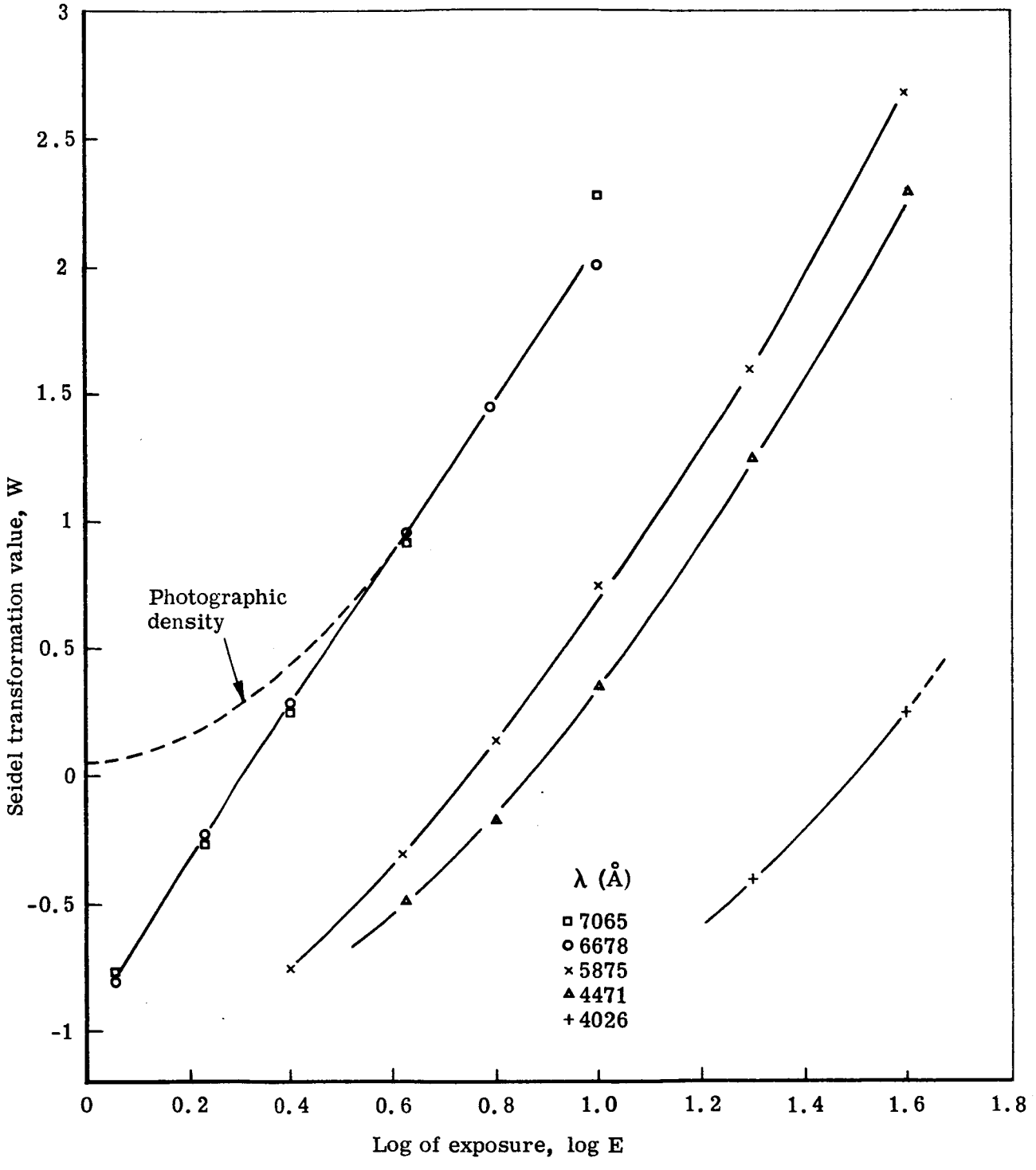

Figure 8. W-log E curves for five wavelengths.

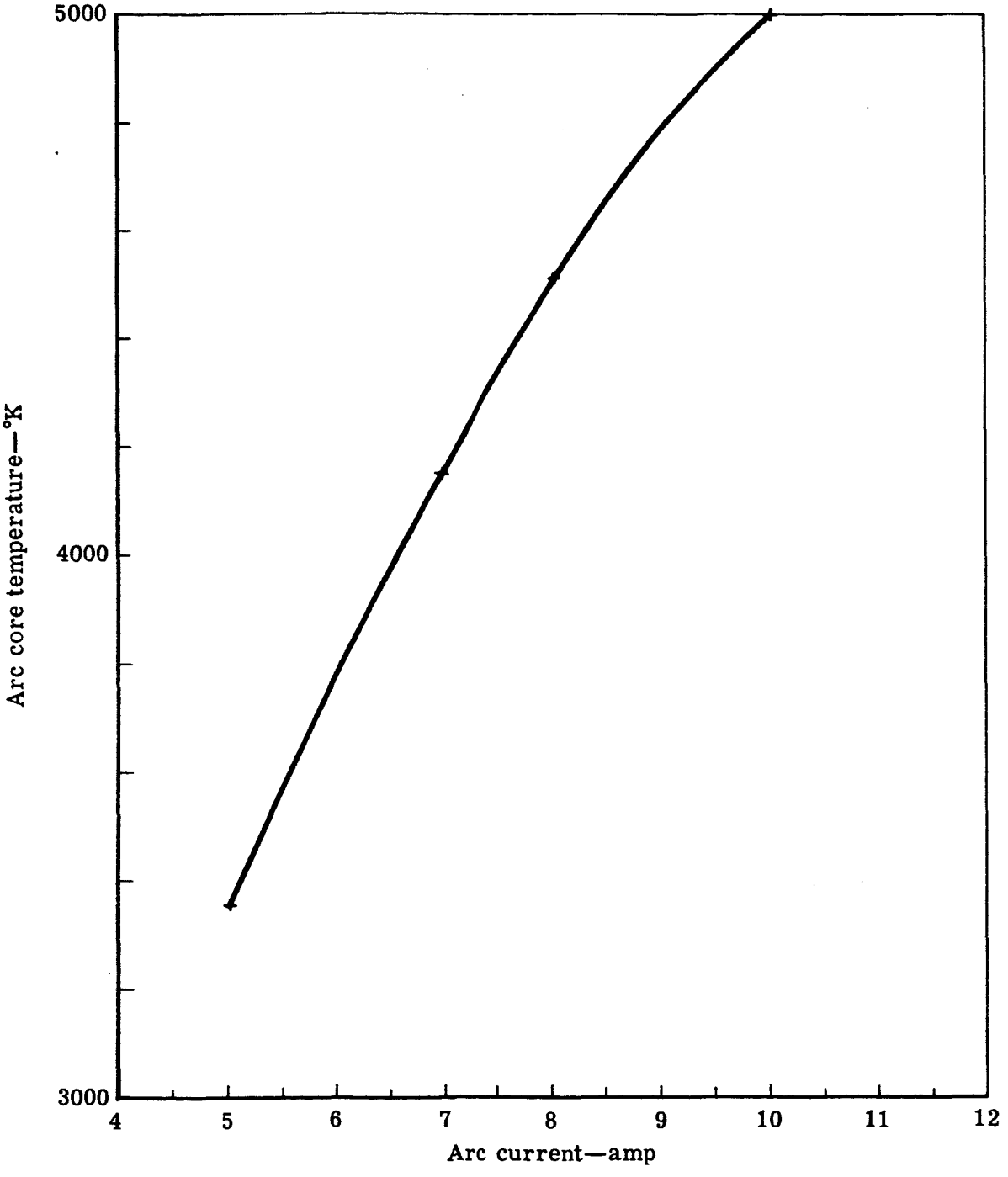

Figure 9. Arc core temperature-current dependency curve.

IV. SPECTRUM PICTURES

METHOD

In the previous section, stigmatic line spectra were evaluated. In this technique, each line constitutes a cross section of the arc. That means that the measured intensity and temperature profile is valid only for that specific cross section.

Of course, it would be most desirable to know the profile of the complete arc. At least, it would be desirable to know how the profile changes from cross section to cross section without being forced to make a new stigmatic spectrum for each possible cross section of the arc. This can be done with the spectrum picture technique. Since this technique is described in detail elsewhere,[10] only a short description is given herein.

Figure 10 is a schematic diagram of the optical arrangement. Axes of the device and entrance slit are parallel (or, in Figure 10, perpendicular to the paper plane). A lens forms an enlarged image of the device in the plane of the entrance slit. A mirror is slowly rotated in the light path. The rotation of this mirror causes the image of the device to move slowly across the entrance slit. Exit slits in the focal plane of the spectrograph are located where spectrum lines of interest appear. Also in the focal plane of the spectrograph is a photographic plate which can be moved slowly in the direction of the dispersion. When the mirror is rotated while the plate is moved, a photographic picture of the device is obtained in the light of one specific spectrum line.

The same setup can also be used to obtain stigmatic line spectra. In this case the motion of photographic plate or film and of the rotating mirror will be stopped and the stigmatic line spectrum photograph will be taken. The plate or film may then be moved a short distance and a new spectrum photograph taken. It is thus possible to accumulate a large number of photographs of the same line on a very small area — e. g., when taking series measurements at different values of arc current. The advantage of this technique is that the entire series may be developed at once, thus reducing errors due to different development procedures. This is demonstrated in Figure 11.

PICTURES WITH HELIUM LINES

Pictures were taken in the light of five different wavelengths: 5878, 7065, 6678, 4471, and 4026Å. Figure 12 shows the excited state for each line originated. The photographs shown in Figures 13, 14, and 15 were taken with three different arc currents as indicated in the

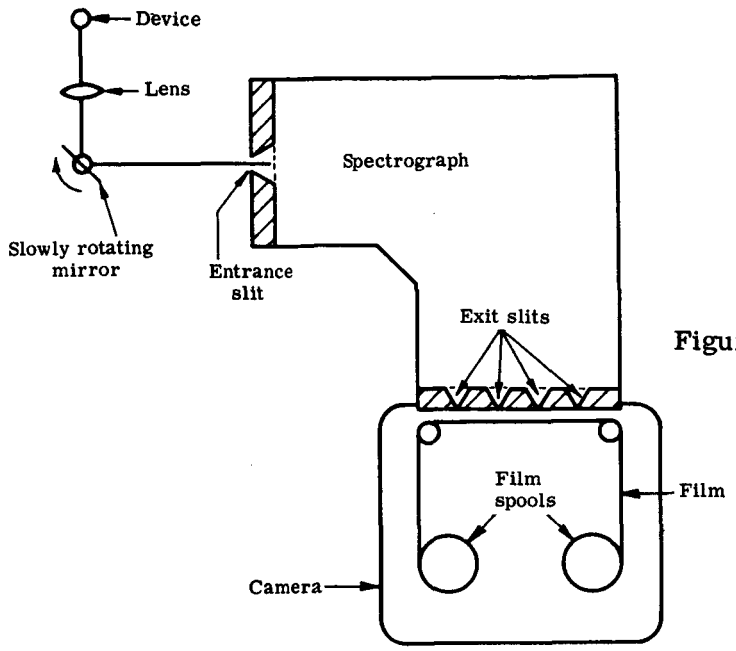

Figure 10. Optical system schematic diagram.

illustrations (6, 8, and 10 amp). The anode is located on the left side of the picture. There are definite changes in the details of the arc; however, this may not be readily apparent because some detail may be lost in the printing process. Starting from the anode on the left side of the photograph, a column extends to the right nearly to the electrode, leaving a dark space between the end of the column and the cathode. This column has a different length for each color. Also, varying arc current changes the length of this column; decreasing the current increases the length of the column.

The sudden changes in arc structure seen in some of the photographs occur when, during the exposure (5 min), the arc jumps to another cathode spot. This phenomenon, which occurs occasionally, may be seen quite easily on the spectrum pictures, but is not detectable on stigmatic line spectra. In the case of stigmatic line spectra, arc jumping would result in an erroneous temperature profile.

This technique will be used to determine the distribution of the cesium seed across the arc. Therefore, at the present time, only photographs of the helium arc without cesium are shown. These photographs will be compared with those taken of the seeded arc.

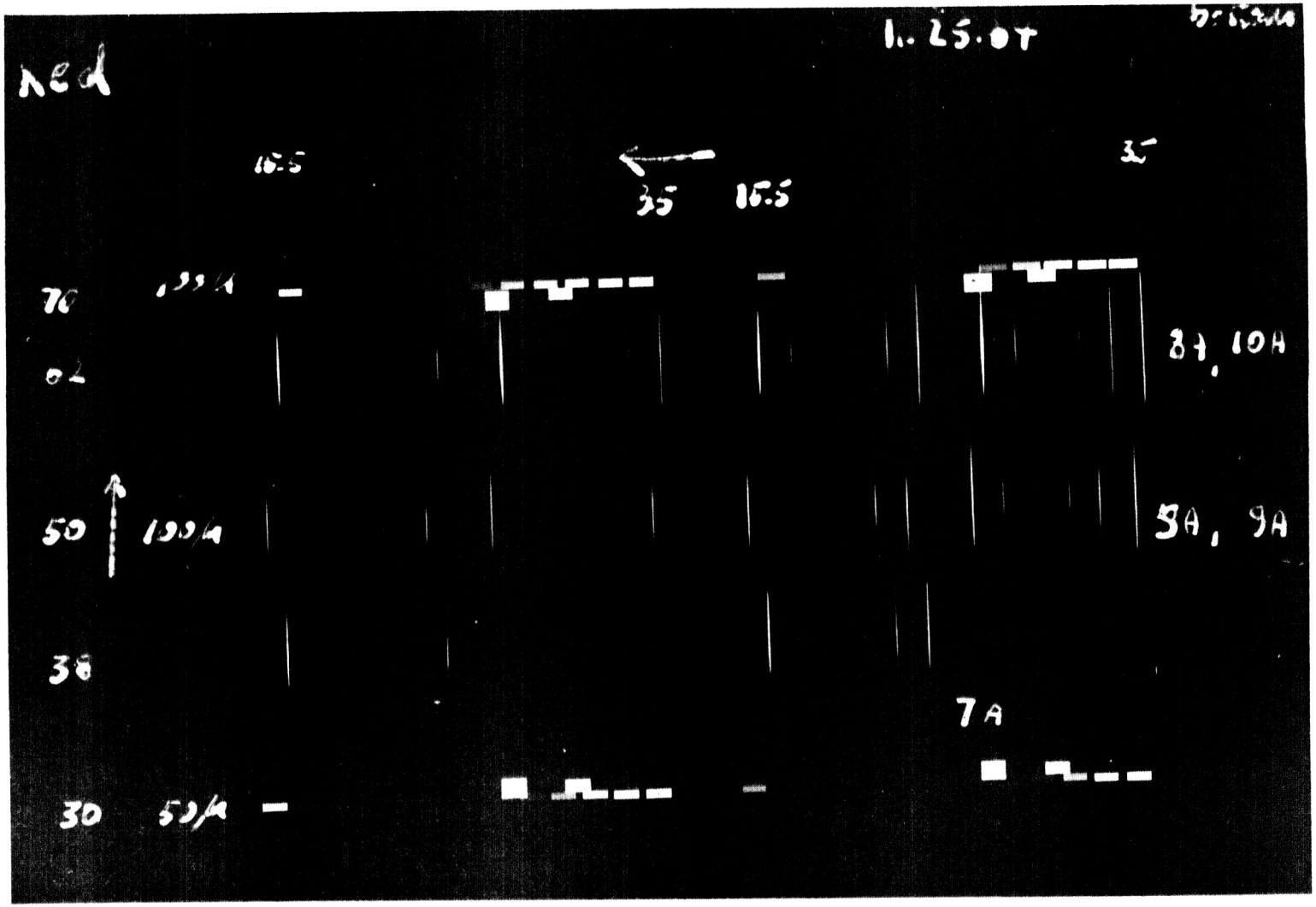

Figure 11. Stigmatic line spectra.

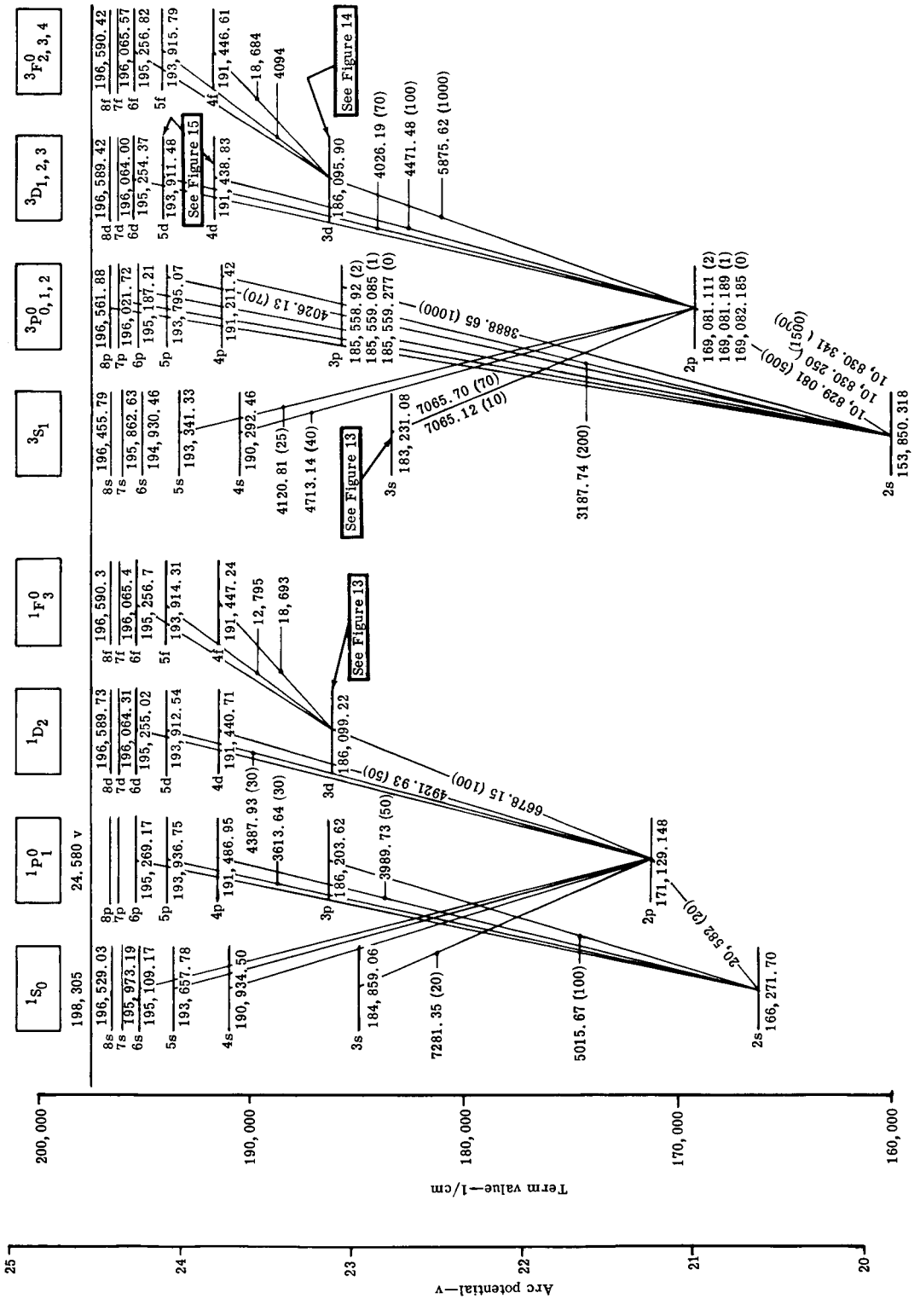

Figure 12. Excited states of helium lines.

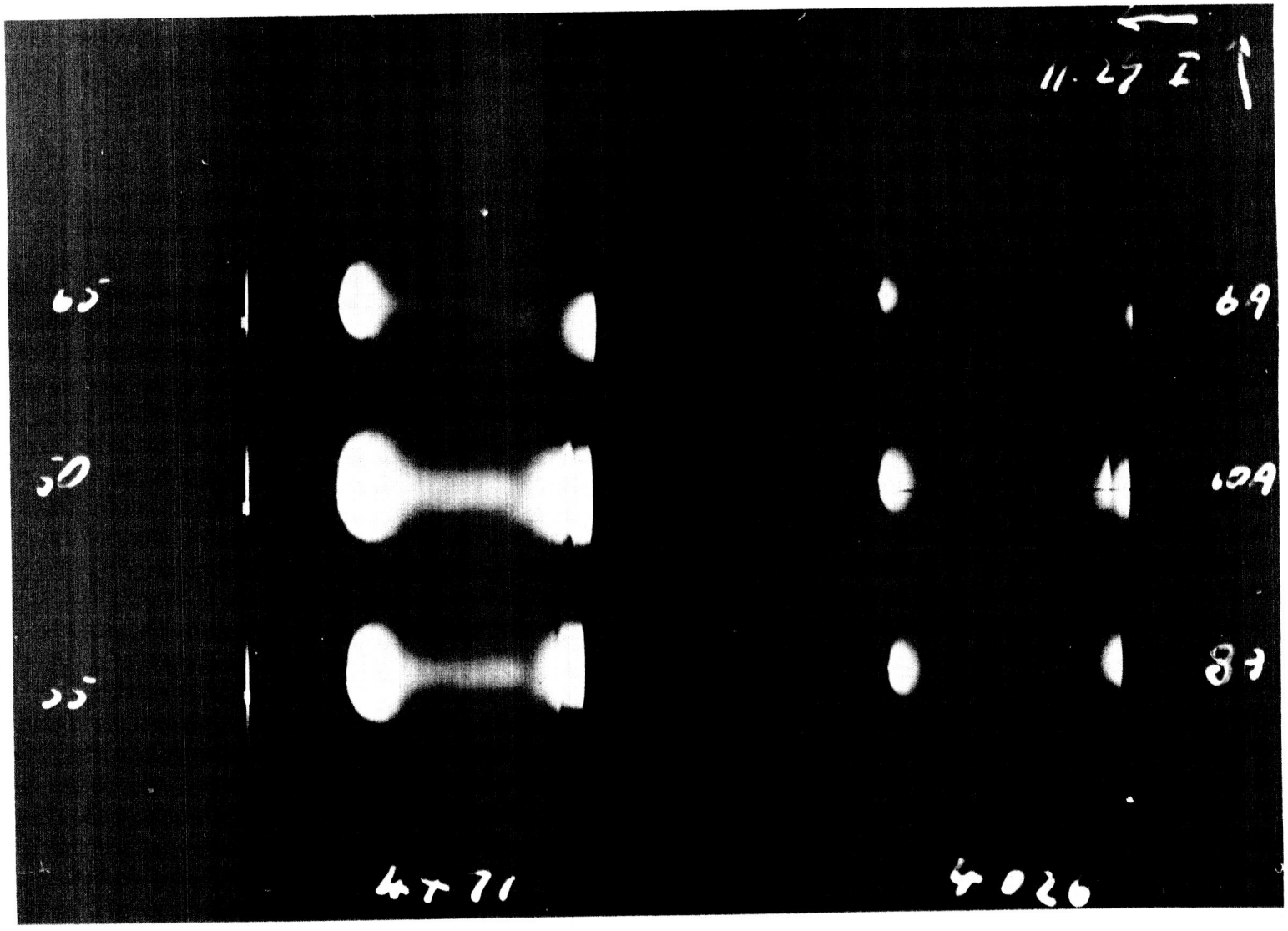

Figure 13. Pictures at 6-, 8-, and 10-amp arc currents and λ = 4471 and 4026 Å.

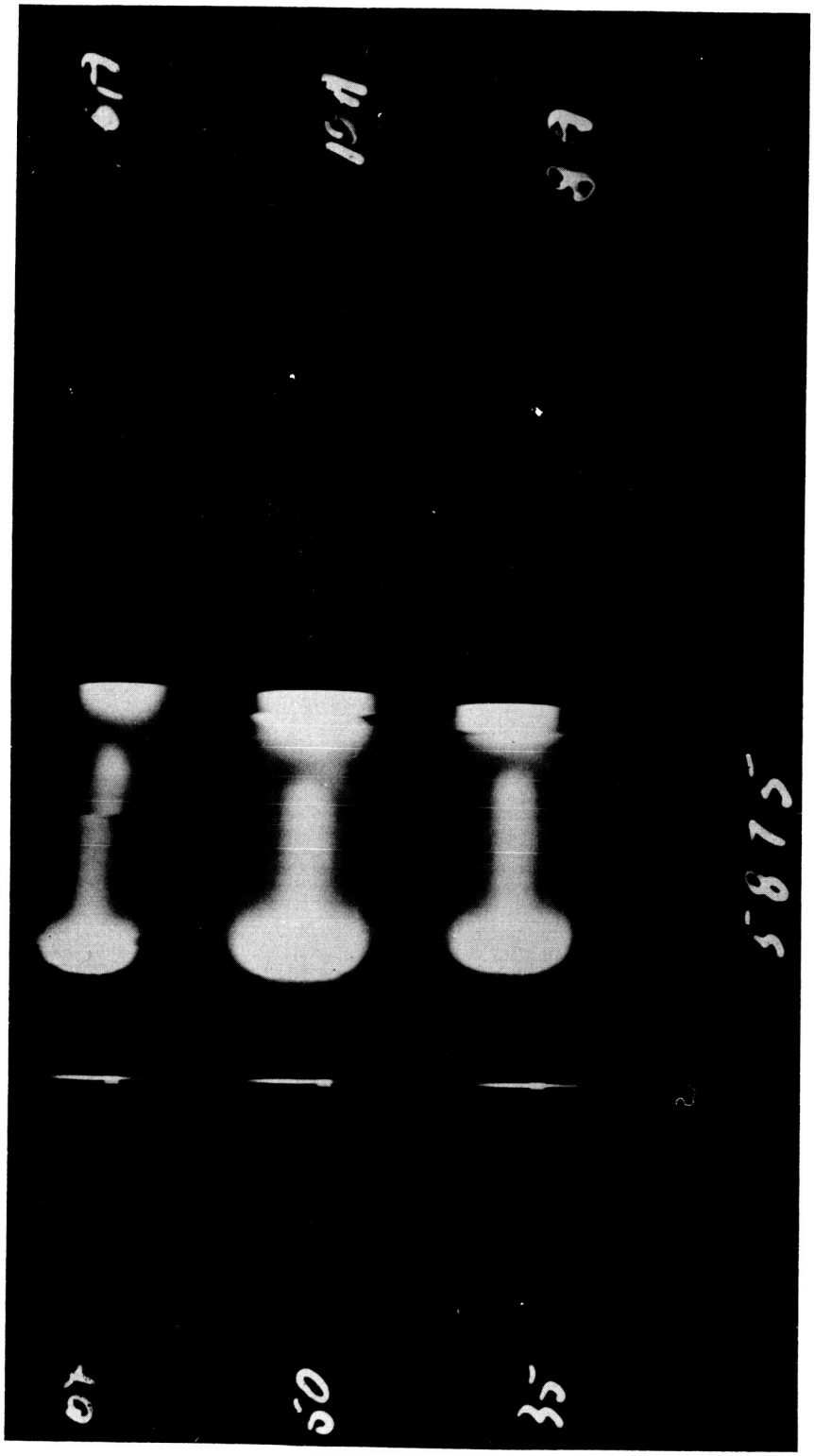

Figure 14. Pictures at 6-, 8-, and 10-amp arc currents and λ = 5875 Å.

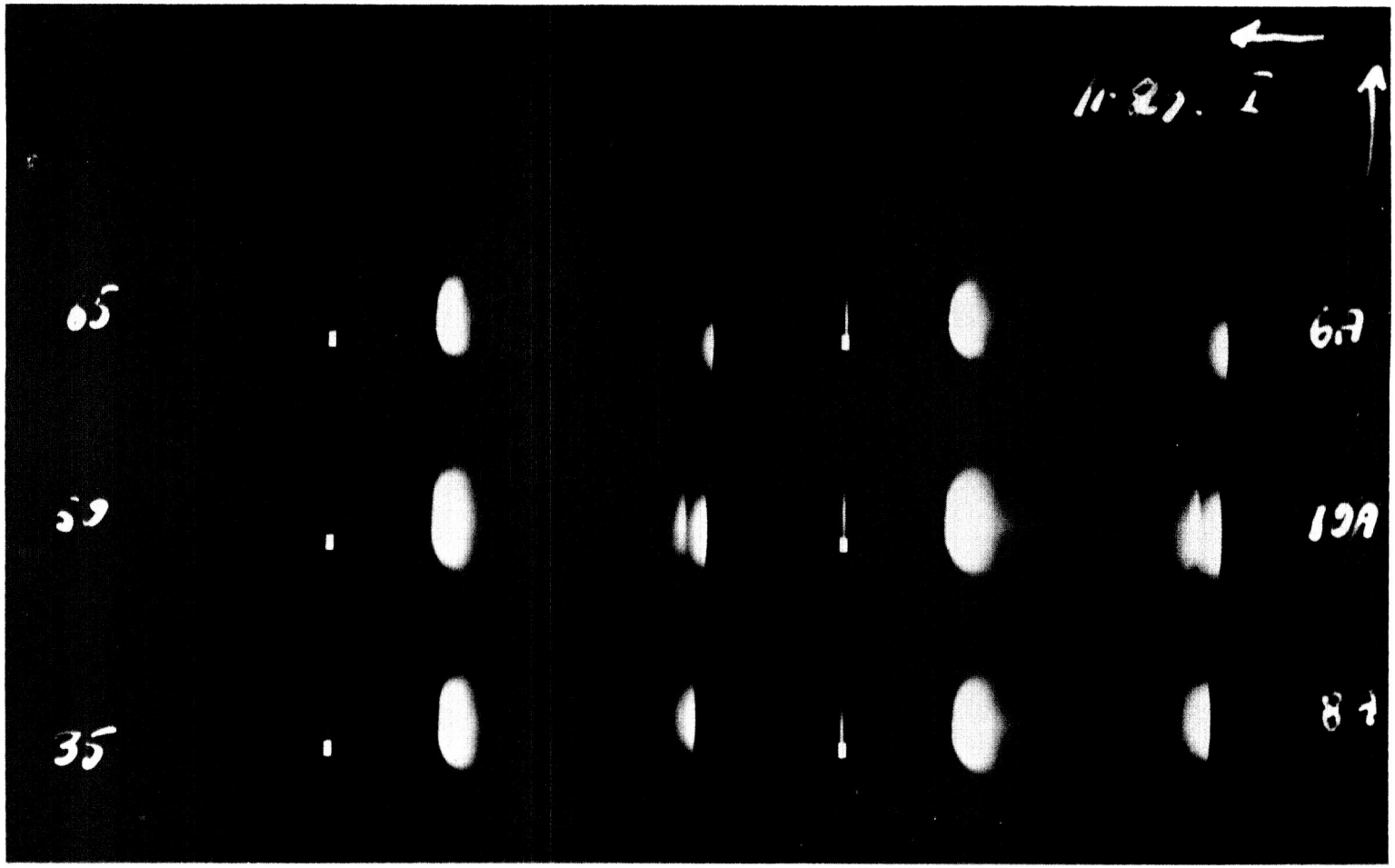

Figure 15. Pictures at 6-, 8-, and 10-amp arc currents and λ = 7065 and 6678 Å.

V. ELECTRONIC INSTRUMENTATION FOR DETECTION OF WEAK SPECTRUM LINES

Spectroscopic data can be recorded either photographically or photoelectrically. Both methods have advantages and disadvantages. The photographic recording yields a two-dimensional picture, one dimension more than the photoelectric recording. The photographic recording is time-integrating. Because of this feature of the photographic plate it is difficult to compare the sensitivity of a photomultiplier. For short-time applications, the photomultiplier offers a clear advantage; for long-time applications, weak lines can be detected photographically which the photomultiplier can never show. Therefore, the ideal device would incorporate a time-integrating circuit and a photomultiplier. Such a device would combine the response linearity of the photocathode and the time-integrating feature of the photographic emulsion.

Since the output of a photomultiplier is a convenient electrical signal, the limitation for amplification is imposed by the noise of the photocathode and other electronic components only. A time-integrating circuit for the photomultiplier would therefore be advantageous only if this circuit is also able to suppress the noise.

Such a circuit was developed and is described subsequently in this section. In the meantime, however, an electronic component called "Enhancetron" (manufactured by Nuclear Data Inc.) became commercially available. The Enhancetron can also be used to suppress circuit noise. During the remainder of the program only the Enhancetron will be used.

Figures 16, 17, and 18 illustrate the Enhancetron technique. Figure 16 shows the intensity profile of a tungsten ribbon taken with a photomultiplier (7102) on the exit slit of the spectrometer and a vibrating mirror on the entrance slit. The output signal of the photomultiplier is amplified and displaced on an oscilloscope. Figure 17 shows the trace when the intensity of the filament is turned down so that the signal is buried in the noise. When the signal of Figure 11 is fed into the Enhancetron and integrated, the result shown in Figure 18 occurs. Parts a, b, c, and d of Figure 18 correspond to different "exposure times"—different integration times. When these photographs were taken, the intensity of the ribbon could no longer be detected with the naked eye. The entrance slit of the spectrometer was only 2 mm high and 5 μ wide.

During the remainder of the program, a more detailed study will be made to compare the sensitivity of typical spectroscopic photographic plates with the "sensitivity" of the photoelectronic technique.

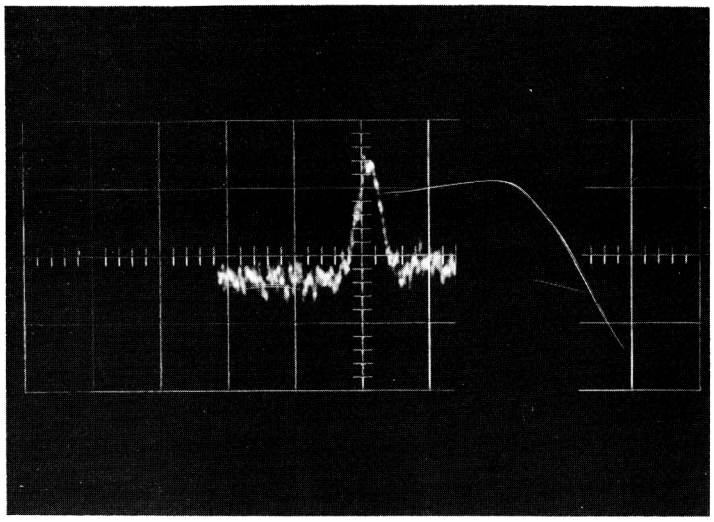

Figure 16. Intensity profile of a tungsten ribbon, taken with a 7102 photomultiplier and a vibrating mirror.

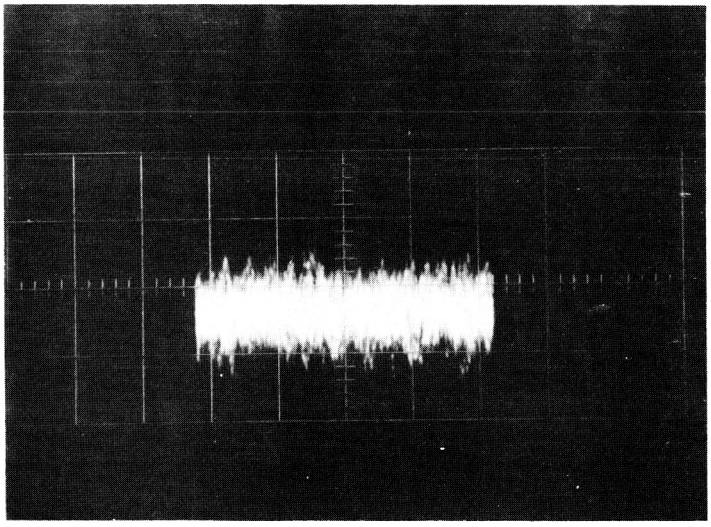

Figure 17. Intensity profile of a tungsten ribbon with the signal buried in noise.

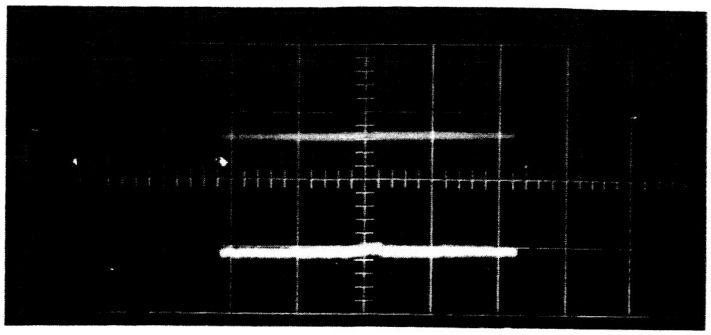

a. 5 sec

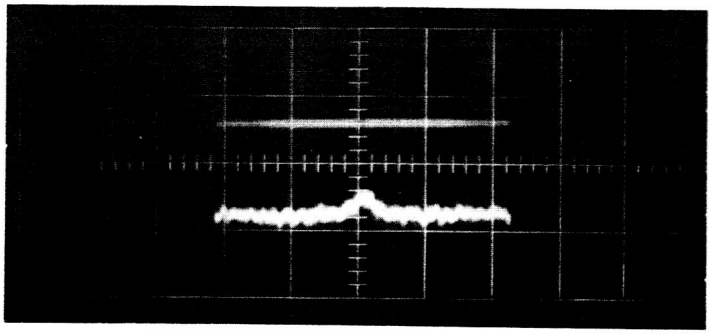

b. 10 sec

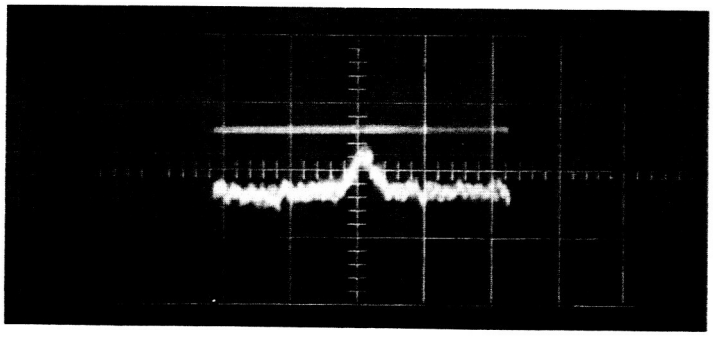

c. 15 sec

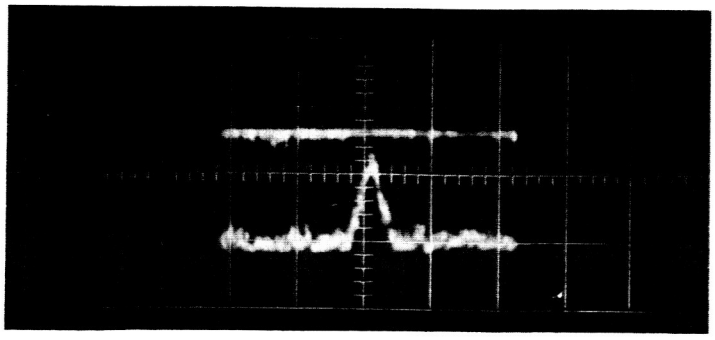

d. 20 sec

Figure 18. Results of applying the Enhancetron to weak signals.

INSTRUMENTATION WITH COMPONENTS COMMONLY AVAILABLE

The following paragraphs describe an electronic device which was developed at Allison and used until the Enhancetron was commercially available. Since the Enhancetron became available, the setup is no longer used but is described herein as a matter of record. Since it produces traces of the same quality as the Enhancetron, it may be applied in all cases in which the application is not extensive enough to justify the procurement of expensive equipment. The instrumentation described herein uses components which are usually available in average laboratories.

Figure 19 shows the conventional method used to detect spectral lines photoelectrically. The pickup triggers the horizontal scan of the oscilloscope at the beginning of each scan of the spectrum by the photomultiplier. Consequently, the spectrum (line profile) is displayed on the oscilloscope.

A definite shortcoming of the system is that the electrical signal developed at the output of the photomultiplier in response to a spectral line may be so weak in relation to the noise generated by the photomultiplier that it cannot be recognized. Consequently, the system of Figure 20 was developed, checked out, and used. The signals appearing at various points of the system are indicated in Figure 21.

Line A of Figure 21 shows the real signal. Signal M corresponds to a prominent spectral line; signal N corresponds to a weak spectral line. Line B indicates how the weak signal can be rendered indiscernible by noise. Only the strong signal is noticeable. An operator using the conventional detection system would never recognize the weak signal.

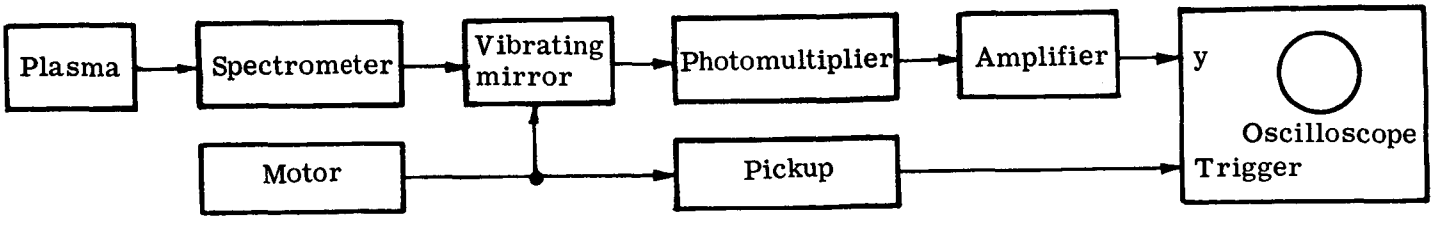

Figure 19. Conventional instrumentation used to obtain spectrographic data.

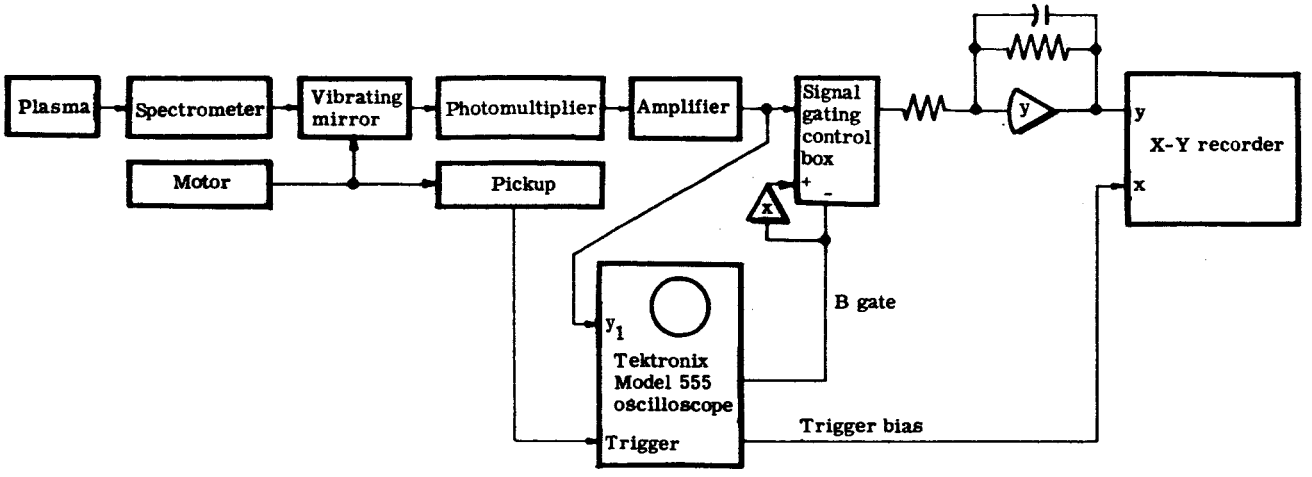

Figure 20. Special instrumentation used to detect weak repetitive signals.

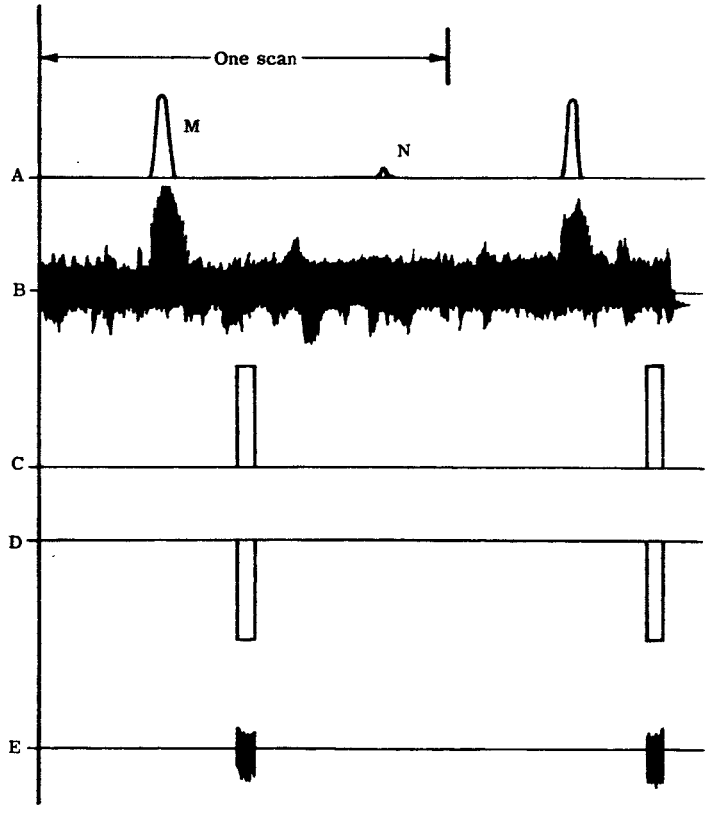

Figure 21. System signals.

The Tektronix Model 555 oscilloscope used is a dual-beam unit. An integral delay system in the oscilloscope permits the B beam to be delayed with respect to the A beam by means of a front panel potentiometer. The system permits a repetitive signal to be displayed on the A trace and any portion of this signal to be selected and displayed on the B trace. The potentiometer which fixes the delay delivers an output voltage which sets the triggering level of a sweep trigger tube. This voltage was taken from the oscilloscope and connected to the x channel of the x-y recorder.

Line C of Figure 21 indicates the gating signal for the B trace. The gate may be varied in width and may be positioned anywhere along the scan.

Line D shows the inverted gate obtained at the output of operational amplifier x.

The circuit of the signal gating control box is shown in Figure 22. During the absence of a gating signal, the output signal from the box is clamped to zero. During the period of a gating signal, the input signal less the d-c component is carried through to the output terminal.

It was found desirable to incorporate a zeroing control into amplifier x. This control was adjusted to bring the output voltage of amplifier x to exactly the same level as the input during the absence of a gating signal. Absence of this control results in a gap between the two voltages, or in an overlap and a consequent large circulating current through the two diodes.

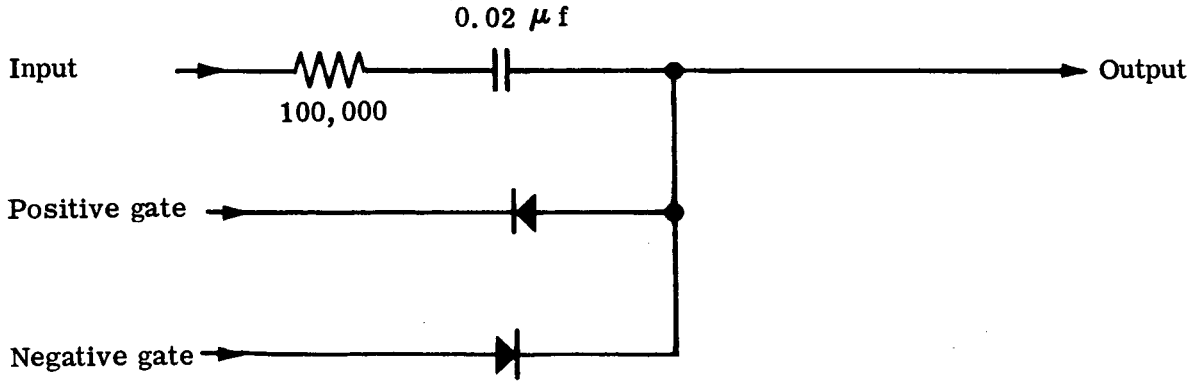

Figure 22. Signal gating control box schematic diagram.

Line E of Figure 21 shows the output of the signal gating control box. The noise burst of line E is an exact replica of the original signal. The noise burst feeds to operational amplifier y— which is adapted to act as a low pass filter. It smoothes out the noise component. It delivers the true signal at the output. When the signal gate is coincident with a buried signal, the output of amplifier y contains the signal plus noise.

The procedure for using the system was as follows.

1. Using the delay control potentiometer on the oscilloscope, search from left to right through one scan. The x-y recorder should move from left to right as the potentiometer is advanced.
2. Repeat the search, this time from right to left. This may be done with pen up or down. The purpose of this search is to disclose any apparent signals which may have occurred due to amplifier drift.

Study of the system will indicate that the base line appearing in Line B of Figure 21 represents the average of all noise plus all true signals in the output of the photomultiplier. Consequently, the presence of a large true signal (or signals) causes an apparent shift in the base line at the output of operational amplifier y. No so-called d-c restoration is provided. Because of these characteristics of the system, signals cannot be detected by adjusting the mirror to one position and leaving it there—causing just one small portion of the spectrum to be fed continuously to the photomultiplier. A scanning technique must be used. The output signal at one point of the spectrum must be compared with the output at other portions.

Some judgment on the part of the operator is required in selecting the time constant for the filter associated with operational amplifier y. If the time constant is too small, the noise output of the amplifier becomes excessive, but the search for signals can be very rapid. If the time constant is too great, noise output is greatly reduced and very weak signals can be detected, but search time must be greatly extended. The extended search time gives rise to troubles from amplifier drift. The question soon arises whether a shift in the output trace is due to a true signal or to drift.

The width of the gate signal should generally be about the same as the width of the true signal being sought. Wider gates tend to smooth the noise but may fail to indicate weak signals. More narrow gates reveal the weak signals but accentuate the noise.

The time required to locate signals can be reduced by reducing the width of scan. However, width of scan should be about five times the width of the electrical signal corresponding to the spectral line sought. It is well to bear in mind that the limit in time reduction is fixed by the signal-to-noise ratio. As the signal becomes weaker, more time must be allowed for a positive identification.

VI. REFERENCES

1. Schneider, R. T. Quarterly Summary Report No. 1—Spectroscopic Investigations of Plasma Properties (11 May—10 August 1964). EDR 3969. Indianapolis: Allison Division, GMC. 9 September 1964.

2. Ibid., pp 15-19.

3. Hörmann, H. "Temperature Distribution and Electron Density in Freely Burning Arcs." Z. Physik. Vol 97 (1935), pp 539-560.

4. Maecker, H. "The Electron Density and Temperature in the Column of a High-Current Carbon Arc." Z. Physik. Vol 136, No. 2 (1953), pp 119-136.

5. Maecker, H. and Peters, T. "Electron Continuum in the Column of the High-Current Carbon Arc and in Other Arcs." Z. Physik. Vol 139 (1954), pp 448-463.

6. Pearce, W.J. "Calculation of the Radial Distribution of Photon Emitters in Symmetric Sources." Conference on Extremely High Temperature. Fischer, H. and Mansur, L. C., ed. New York: John Wiley and Sons, 1958, p 123.

7. Hattenburg, A. T. and Kostkowski, H. T. "Experimental Proof of the Absence of Equilibrium in a Helium Arc." Temperature, its Measurement and Control in Science and Industry. C. M. Herzfeld, editor-in-chief. Vol 3, Part 1. Basic Concepts, Standards and Methods. F. G. Brickwedde, ed. New York: Reinhold Publishing Corp, 1963, p 587.

8. Burns, J. Research on the Effects of Arc Fluctuations on Spectroscopically Determined Temperatures in Arc Plasmas, Third Quarterly Progress Report. Chicago: University of Chicago, Laboratory for Applied Sciences. February 1964, p 6.

9. Honerjäger-Sohm, M. and Kaiser, H. "Correction for Background in the Measurements of Intensity Ratios." Spectrochim. Acta. Vol 2 (1944), pp 396-416.

10. Schneider, R. T. "A Spectroscopic Method Allowing Spatial Resolution." Proceedings, Sixth International Conference on Ionization Phenomena in Gases. Paris, 8-13 July 1963.